

DRAFT: November 13, 2017

Ion-by-Ion Differential Emission Measure Determination of Collisionally Ionized Plasma: I. Method

Patrick S. Wojdowski and Norbert S. Schulz

Center for Space Research, Massachusetts Institute of Technology

pswoj@space.mit.edu

ABSTRACT

We describe a technique to derive constraints on the differential emission measure (DEM) distribution, a measure of the temperature distribution, of collisionally ionized hot plasmas from their X-ray emission line spectra. This technique involves fitting spectra using a number of components, each of which is the entire X-ray line emission spectrum for a single ion. It is applicable to high-resolution X-ray spectra of any collisionally ionized plasma and particularly useful for spectra in which the emission lines are broadened and blended such as those of the winds of hot stars. This method does not require that any explicit assumptions about the form of the DEM distribution be made and is easily automated.

1. Introduction

The X-ray emission for a large class of astrophysical objects is dominated by emission from a hot, thin plasma in which the electrons have a thermal velocity distribution and ion-electron recombination is balanced by collisional ionization — i.e., collisional ionization equilibrium. This class of astrophysical objects includes both hot and cool stars, clusters of galaxies, and elliptical galaxies as well as some cataclysmic variable systems and active galactic nuclei (see, e.g., Paerels & Kahn 2003). A large class of laboratory plasmas are also in collisional ionization equilibrium. At temperatures above $\sim 10^6$ K, plasmas in collisional ionization equilibrium emit X-rays in the 1.5–30 Å (0.4–8 keV) band. Up to temperatures of $\sim 3 \times 10^8$, that X-ray emission is characterized by strong line emission. This line emission varies strongly with temperature changes of a few tenths of a decade or more.

The unprecedented ability of the grating spectrometers on the *Chandra* and *XMM-Newton* observatories to resolve this X-ray line emission present new possibilities for measuring temperatures of plasmas in CIE and, therefore, new tests of theories of astrophysical

objects. Compilations of X-ray line emissivities have long been available (e.g., Raymond & Smith 1977, Mewe, Gronenschild, & van den Oord 1985, Smith et al. 2001) and given a detailed model of an astrophysical object, it is, in general, straightforward to compute the emission line spectrum of any optically thin CIE plasma. For the purpose of determining luminosities of most emission lines, the three dimensional temperature and density distributions may be reduced to the differential emission measure (DEM) distribution, a single-valued function of temperature which we define in §2. However, it is often the case that no explicit theoretical prediction exists for the DEM distribution of objects of interest. Furthermore, even when theory does provide an explicit prediction of the differential emission measure, it is often desirable to make measurements of the differential emission measure without respect to any model. Therefore, in this paper, we develop a method for obtaining constraints on the DEM distribution of a collisionally ionized plasma from its X-ray emission line spectrum without respect to any physical model.

Our method consists of fitting the observed spectral data using a model consisting of a continuum plus a number of line emission components, with each line emission component containing all of the lines of a single ion in the observed wavelength band. Since each ion emits only in a specific temperature range, the best fit magnitude for the line emission of a given ion gives a measure of a weighted average of the DEM distribution in that temperature range times the abundance of that element. We plot the constraints for all of the ions as a function of the temperature at which emission from the ion peaks. These plots may be understood as one-dimensional “images” of the DEM distributions in that they consist of discrete “pixels” (one for each ion) and differ from the true DEM distribution by a convolution which may be understood as a “temperature-spread” function. In addition, by fitting the entire X-ray spectrum, rather than attempting to measure fluxes of individual lines, we take advantage of the information available from blended lines. This is particularly important in the analysis of spectra in which the lines are significantly broadened and blended due to insufficient instrumental spectral resolution, Doppler motion of the emitting plasma, or other effects. This method can be automated, facilitating the analysis of large numbers of spectra. This attribute will become increasingly important with the future *Constellation-X* mission which will be able to obtain high-resolution spectra for a large number of objects. While we are unaware of any use of this method exactly as it is described here, it is quite similar to and, in fact, inspired by methods described and applied by Pottasch (1963) for the analysis of solar ultraviolet spectra, by Sako et al. (1999) for the analysis of an X-ray spectrum of the photoionized wind of the high mass X-ray binary Vela X-1, and by Brinkman et al. (2001) and Behar, Cottam, & Kahn (2001) for analyses of the X-ray spectra of the corona of the cool stars HR 1099 and Capella, respectively.

In §2 we motivate and describe our method in detail and in §3, we apply it to a simulated

spectrum of a plasma with a continuous temperature distribution and simulated spectra of several single temperature plasmas. In §4, we discuss the possible applications of our method. The X-ray emission of most hot stars originates in supersonic stellar winds, resulting in broadened and blended emission lines. Therefore, our technique is particularly useful in the analysis of these spectra and in a companion paper (hereafter, “Paper II”) we apply our technique to spectra of nine hot stars.

2. The Differential Emission Measure Distribution and its Determination

In a plasma in CIE, line emission is due primarily to electron-ion collisional excitation. Therefore, at low densities, for a given temperature, line emissivities are proportional to the square of the density. However, at high enough density, ions in some metastable excited states may undergo additional collisional excitation, resulting in the emissivities of some lines depending on higher powers of the density. By definition, in a plasma in CIE, the radiation field is too weak to affect the ionization balance. However, there is a regime in which a plasma may be in CIE but in which the radiation field is strong enough to induce further excitation of ions in metastable excited states. This leads to additional dependence of the line emissivities on the radiation intensity.

For simplicity, in §2.1, we define the DEM distribution and describe a method for deriving constraints on it from its X-ray emission spectrum for a plasma in which excited ions do not undergo further excitation. Then, in §2.2, we describe a modified version of this method for deriving constraints on the DEM distribution of plasmas in which ions in metastable excited may undergo further excitation.

2.1. Low Density and Radiation Intensity

In the limit of low density and low radiation intensity, at a given temperature, line emissivities depend on the square of the density. Therefore, for the purpose of determining the emission line spectrum, the three dimensional temperature and density distributions may be reduced to the DEM distribution defined as:

$$\mathcal{D}(T) \equiv \frac{dE}{d\log T} \quad (1)$$

where T is the electron temperature and E is the emission measure defined as

$$E(T) \equiv \int_0^T n_e n_H dV \quad (2)$$

where n_e is the electron density, n_H is the hydrogen atom density and the integration is over that volume where the temperature is less than T . In addition, because diffuse plasmas in collisional ionization equilibrium cool radiatively, the cooling of gas is also determined by the DEM distribution. Therefore, constraints on the DEM distribution provide constraints on the overall energetics of the X-ray emitting plasmas.

The luminosity of an emission line i from an ion of charge state z of element Z may be expressed as

$$L_{Z,z,i} = A_Z \int \mathcal{D}(T) P_{Z,z,i}(T) d \log T \quad (3)$$

where A_Z is the abundance of element Z relative to solar and $P_{Z,z,i}(T)$ is the line power function. The line power function depends only on atomic physics parameters and the solar abundance of the element. Its variation with temperature is due to the variation of the fractional abundance of the emitting ion as well as the variation of intrinsic collisional excitation rates. Line power functions have been tabulated for a large number of lines. Therefore, from the measurement of a line luminosity, a constraint on the product of the elemental abundance and the DEM distribution can be inferred.

In the absence of specific theoretical predictions of DEM distributions, it may be useful to determine, at least approximately, the magnitude and form of the DEM distribution. If we divide Equation 3 by $\int P_{Z,z,i}(T) d \log T$, then it may be seen that the measurement of a line luminosity constrains the product of an elemental abundance and a “weighted average” of the DEM distribution. In Figure 1, we show the power functions of the lines of two ions. The line power data we use in this figure and elsewhere in this paper is from a version of Astrophysical Plasma Emission Database (APED, Smith et al. 2001) based on the publicly released version 1.1 but modified to include the dependence of the line power functions on density (R. Smith, private communication 2002). The grid for the database we use is somewhat sparse: line powers are tabulated for ten temperature values per decade and two density values per decade. It may be seen in the figure that the line power functions are single-peaked and, compared to their peak values, are negligible outside of temperature ranges of about one decade around each peak. Therefore, the weighted average values of the DEM that we obtain from the measurement of line luminosities are, approximately, the average value of the DEM in the vicinity of the peak of that line’s power function.

Measuring the luminosities of several lines with power functions that peak at different temperatures gives us approximate average values of the DEM distribution in several temperature ranges. However, for many applications, it may be difficult to measure luminosities of individual lines as they may be blended owing either to the finite spectral resolution of the instrument or intrinsic line broadening. In order to avoid the uncertainties related to the measurement of fluxes of individual lines, we take advantage of the fact that the power

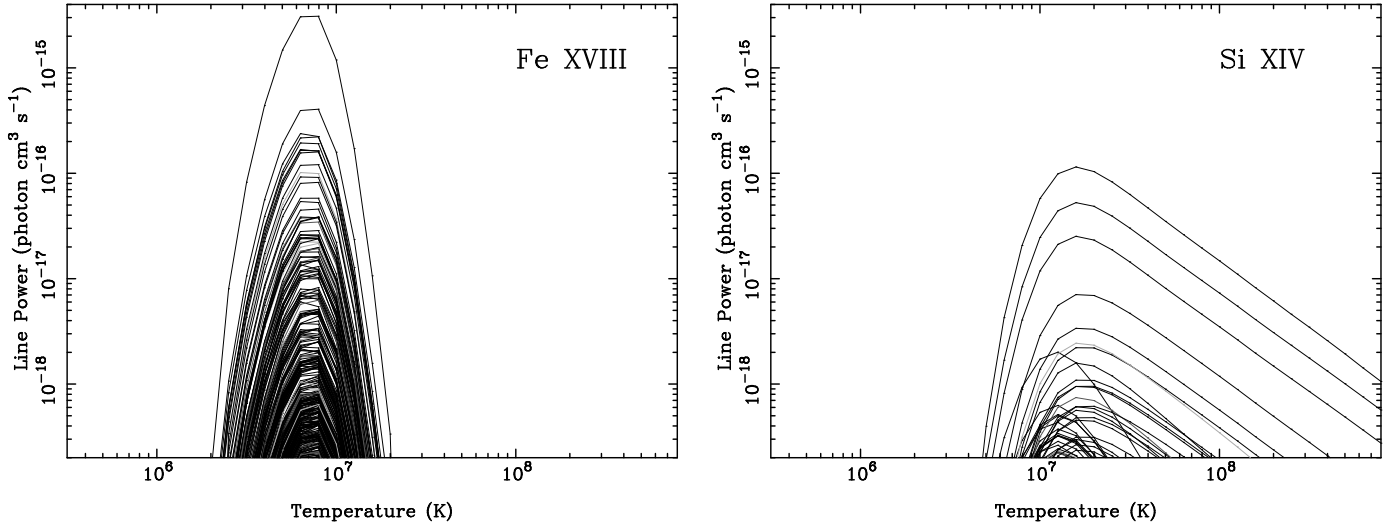


Fig. 1.— Line power functions and summed line power functions for the L -shell ion Fe XVIII and the hydrogen-like ion Si XIV. The topmost curve in each panel is the total line power function (Θ , defined by Equation 4). All lines from the database are plotted. For Fe XVIII, the lines can be seen to have nearly the same temperature dependence. For Si XIV, a family of line power functions have a temperature dependence significantly different from the others, peaking at a lower temperature. However, the peak values of these line power functions are only a few percent of those of the strongest lines. These figures illustrate the validity of our approximation that the line power functions of most of the lines of a given ion, and all of the strongest lines of that ion, the line power functions have almost the same shape. The sparseness of the temperature grid is evident from the jagged appearance of the curves.

functions of most of the lines, and all of the strong lines, of an ion have very nearly the same shape. This similarity of line power functions is demonstrated in Figure 1. If two lines have power functions that have the same shape but differ by a constant factor, then the ratio of the luminosities of those two lines will differ by that same constant factor regardless of the DEM distribution. Therefore, instead of attempting to measure the fluxes of individual emission lines in a spectrum, we fit the entire spectrum using all of the lines in the database, constraining the line fluxes such that ratios of the line fluxes for any individual ion are fixed. In such a fit, there is only one free line luminosity normalization parameter for each ion. Just as the luminosities of individual lines imply average values of the DEM distribution in temperature ranges defined by the line power functions, so do these normalization parameters. However, because each ion has a distinct set of lines with distinct luminosity ratios, these normalization parameters and the corresponding average values of the DEM distribution can be uniquely constrained, even if lines are significantly blended. For several ions, there is a family of lines, the dielectronic recombination lines, that have power functions that differ significantly from the other lines of the ion. This fact can be seen in Figure 1 for Si XIV. However, the dielectronic lines are quite weak. The peak powers of the dielectronic recombination lines are only a few percent of those of strongest lines. Therefore, we proceed with our attempt to derive constraints on DEM distributions by fitting spectra with fixed line luminosity ratios.

In order to choose line luminosity ratios for fitting spectra, we define the function $\Theta_{Z,z}$ for each ion as the sum of all of the power functions for all of the lines of that ion:

$$\Theta_{Z,z}(T) \equiv \sum_i P_{Z,z,i}(T). \quad (4)$$

For each function Θ , we define a temperature T_p to be the temperature at which it peaks. We then let the line luminosities be given by

$$L_{Z,z,i} = D_{Z,z} P_{Z,z,i}(T_{p,Z,z}) \Delta \log T_{Z,z} \quad (5)$$

where $D_{Z,z}$ is a variable normalization parameter and

$$\Delta_{Z,z} \log T \equiv \frac{\int \Theta_{Z,z}(T) d \log T}{\Theta_{Z,z}(T_{p,Z,z})}. \quad (6)$$

In Table 1 we give values of T_p and the quantities $\Delta_- \log T$ and $\Delta_+ \log T$, defined as

$$\Delta_- \log T_{Z,z} \equiv \frac{\int_0^{T_{p,Z,z}} \Theta_{Z,z}(T) d \log T}{\Theta_{Z,z}(T_{p,Z,z})}, \quad (7)$$

$$\Delta_+ \log T_{Z,z} \equiv \frac{\int_{T_{p,Z,z}}^{\infty} \Theta_{Z,z}(T) d \log T}{\Theta_{Z,z}(T_{p,Z,z})} \quad (8)$$

for each of the ions we use in our analysis. The quantities $\Delta_- \log T$ and $\Delta_+ \log T$ provide an indication of the temperature ranges over which the ions have significant line emission.

The fact that several ions have the same value of T_p is an artifact of the sparse temperature grid.

If all of the line power functions of a given ion have exactly the same shape, then the value of D for that ion gives the product of the elemental abundance and the average of the DEM distribution weighted by that ion’s function θ as described above for individual lines. As mentioned above, not all of the line power functions for every ion have the same shape. However, as those line power functions that differ significantly have magnitudes of only approximately 1% of the value of the strongest line power functions, we expect an error due to the difference of line power functions of no more than about 1%.

2.2. Line Pumping

As we have mentioned before, some ions have metastable excited states that are susceptible to further excitation by collisions with electrons or absorption of photons. The result of this is that the emission in lines resulting from the decay of the metastable state are “pumped” into other lines. We first consider pumping by collisional excitation because the effects of the two mechanisms are similar and because data for pumping by collisional excitation is more readily available. For this case, the line emission may still be described by line power functions. However, the line power P is a function of density as well as temperature. Therefore, the emission line spectrum depends on the two-dimensional temperature-density DEM

$$\mathcal{H}(T, n_e) \equiv \frac{d^2 E}{d \log T d \log n_e} \quad (9)$$

The DEM distribution is related to this quantity by

$$\mathcal{D}(T) = \int \mathcal{H}(T, n_e) d \log n_e. \quad (10)$$

If the density dependence of each line power function of a single ion is due to a single upward transition from a single metastable state and the collisional excitation rate for that transition does not change much over the temperature range where that ion emits, then the line power functions for that ion may be well approximated by the form

$$P_{Z,z,i}(T, n_e) = \Theta_{Z,z}(T)(B_{Z,z,i} + F_{Z,z,i}H_{Z,z}(n_e)) \quad (11)$$

where Θ and H are functions that are the same for all of the lines of a given ion and B and F are constant coefficients for each line. Even if the two conditions mentioned above are not

Table 1. Temperature Data for Ion Line Power Functions

| Ion | $T_p(\text{K})$ | $\Delta_- \log T$ | $\Delta_+ \log T$ |
|----------|-------------------|-------------------|-------------------|
| N VI | 1.6×10^6 | 0.20 | 0.34 |
| N VII | 2.0×10^6 | 0.14 | 0.34 |
| O VII | 2.0×10^6 | 0.16 | 0.21 |
| O VIII | 3.2×10^6 | 0.18 | 0.34 |
| Ne IX | 4.0×10^6 | 0.22 | 0.19 |
| Ne X | 6.3×10^6 | 0.23 | 0.35 |
| Mg XI | 6.3×10^6 | 0.22 | 0.22 |
| Mg XII | 1.0×10^7 | 0.20 | 0.40 |
| Si XIII | 1.0×10^7 | 0.24 | 0.23 |
| Si XIV | 1.6×10^7 | 0.21 | 0.42 |
| S XV | 1.6×10^7 | 0.30 | 0.22 |
| S XVI | 2.5×10^7 | 0.24 | 0.43 |
| Ar XVII | 2.0×10^7 | 0.25 | 0.28 |
| Ar XVIII | 4.0×10^7 | 0.28 | 0.42 |
| Ca XIX | 2.5×10^7 | 0.24 | 0.33 |
| Ca XX | 5.0×10^7 | 0.23 | 0.48 |
| Fe XVII | 5.0×10^6 | 0.18 | 0.21 |
| Fe XVIII | 7.9×10^6 | 0.21 | 0.10 |
| Fe XIX | 7.9×10^6 | 0.11 | 0.15 |
| Fe XX | 1.0×10^7 | 0.13 | 0.11 |
| Fe XXI | 1.0×10^7 | 0.08 | 0.18 |
| Fe XXII | 1.3×10^7 | 0.11 | 0.15 |
| Fe XXIII | 1.6×10^7 | 0.16 | 0.17 |
| Fe XXIV | 2.0×10^7 | 0.18 | 0.32 |
| Fe XXV | 6.3×10^7 | 0.33 | 0.33 |
| Fe XXVI | 1.3×10^8 | 0.28 | 0.48 |

satisfied, the line power functions may be well approximated by this form. We discuss the validity of this assumption in §2.2.1 and proceed here with the assumption that the power functions have this form.

We define the functions Θ , and the temperatures where they peak, T_p , as before in the limit of low density and low radiation intensity. With this definition, the functions $H(n_e)$ go to zero as n_e does. If the functions H are continuous, it is possible to show that for any temperature-density DEM distribution $\mathcal{H}(T, n_e)$ with an associated DEM distribution $\mathcal{D}(T) = \int \mathcal{H}(T, n_e) d \log n_e$, there exists, for each ion, a value of the density $n'_{Z,z}$ such that the temperature-density DEM distribution $\mathcal{H}'_{Z,z}$ defined as

$$\mathcal{H}'_{Z,z}(T, n_e) \equiv \mathcal{D}(T) \delta(n_e - n'_{Z,z}) \quad (12)$$

produces the same luminosities for all of the emission lines of the ion Z, z as does $\mathcal{H}(T, n_e)$. Therefore, we modify the method described above by adopting the variable parameters $n'_{Z,z}$ and let the line luminosities be

$$L_{Z,z,i} = D_{Z,z} P_{Z,z,i}(T_{p,Z,z}, n'_{Z,z}) \Delta_{Z,z} \log T \quad (13)$$

where $\Delta_{Z,z} \log T$ is defined as before in Equation 6. That is, we fit the entire spectrum using all of the lines in the database as described in §2.1. However, instead of constraining the line flux ratios of individual ions to be fixed, we allow the ratios to vary with a density parameter $n'_{Z,z}$ for that ion. The density parameters for each of the ions are allowed vary independently. Again, $D_{Z,z}$ approximates the product of the elemental abundance and the average of the DEM distribution weighted by $\Theta_{Z,z}(T)$. Even if equation 11 is not satisfied, this method will result in good fits to the data and accurate constraints on the DEM distribution if the emitting plasma has a single density or if density and temperature are strongly correlated within the plasma.

2.2.1. Accuracy of the Power Function Approximation

A systematic study of the density dependence of emission lines with wavelengths from 1.2–31 Å has been undertaken by Smith et al. (2002). These authors have made fits to the line powers as functions of density at the constant temperatures 10^6 , $10^{6.5}$, 10^7 , and $10^{7.5}$ K for lines with peak powers exceeding a minimum value and also meeting a criterion for variability with density at each temperature. They found the power functions of most of the lines satisfying those criteria ($\sim 90\%$) could be approximated well using a function of the form

$$P(n_e) = c_0 + c_1 \exp(-n_e/n_1) \quad (14)$$

where c_0 , c_1 , and n_1 are fit parameters. If the density dependence for the line powers of all of the lines of an ion have the form of Equation 14, then Equation 11 is a valid description of the line power functions if, in the temperature range where line emission is significant,

- all of the lines of any one ion have the same value of n_1 and
- for any single line, the ratio of the line power at high density (c_0) to the value at low density ($c_0 + c_1$) and the value of n_1 do not change with temperature.

We have inspected the results of Smith et al. (2002) and found that, for all of the ions we use except Fe XIX, Fe XX, and Fe XXI, most of the lines ($\sim 90\%$) are described by Equation 14 and have values of n_1 that are very close, having a standard deviation of 0.1 or less in $\log n_1$. For those lines, of any ion, that meet the criteria to be fit at more than one temperature, the root mean square (RMS) of the difference between values of $\log n_1$ for the same ion at different temperatures is 0.09 and the RMS of the difference between values of $\log(c_0/(c_0 + c_1))$ is 0.16. In summary, Equation 11 is not exactly satisfied for all ions. However, because most line power functions do not depend on density, it is unlikely that this would cause errors greater than a factor of a few. Because Equation 11 is near to being satisfied for most ions, we expect the actual errors to be much less: not much greater than 10 or 20%.

2.2.2. Radiation

Because metastable states may be photoexcited, line powers are functions not only of temperature and density but also of the mean radiation intensity at the frequencies of the transitions that affect line emission. That is, the line power may be written $P_{Z,z,i}(T, n_e, J_\nu)$ or $P_{Z,z,i}(T, n_e, J_{\nu_{i1}}, J_{\nu_{i2}}, \dots, J_{\nu_{im}})$ where J_ν is the mean radiation intensity as a function of frequency and $J_{\nu_{ij}}$ are the mean radiation intensities at the frequencies of the transitions affecting line i . While this is, in principle, a large number of variables, the number of transitions in which photoexcitation plays a significant role (the value of m) is often only one. Furthermore, for a given system, the values of $J_{\nu_{ij}}$ may be a function of a small number of variables. For example, in hot star winds, the radiation intensity due to the stellar photosphere is given by

$$J_\nu = I_{\star,\nu} W \tag{15}$$

where $I_{\star,\nu}$ is the radiation intensity at the surface of the star and is approximately that of a blackbody with a temperature, depending on the stellar type, of a few tens of thousand K and W is a factor accounting for the geometrical dilution of the stellar radiation with

distance from the star. We know of no systematic study (at least, not of the scope of that by Smith et al. 2002 for density) of the dependence of line powers on radiation. However, as radiation and density both affect the line power through excitation of metastable stable states, the effects are similar. Therefore, we use the method described above — we take the line emission from each ion to be determined by the temperature at which its emission peaks and a density which is a free parameter, independent of the density values of the other ions — and assume that the effects of radiation and density can be replicated approximately by density alone. In Paper II we again address the validity of this approach for plasmas with a significant pumping radiation field.

3. Tests with Simulated Data

3.1. Simulations

In order to demonstrate the performance of our model, we tested our method by applying it to a series of simulated spectra. We simulated *Chandra* MEG and HEG spectra for a plasma with a DEM distribution constant with temperature over the range 3.2×10^5 – 7.9×10^8 K¹ and zero elsewhere. We also simulated spectra from single-temperature plasmas at the temperatures 3×10^5 , 10^6 , 3×10^6 , 10^7 , 3×10^7 , 10^8 , and 3×10^8 K. In Paper II we apply our method to spectra of hot stars. Therefore, for our simulations we adopt the parameters of ζ Pup, the best-studied hot star in the X-ray band, and of an observation of it with *Chandra* (see Paper II). However, the results of the application of our method to these simulated data indicate the general behavior of our method.

To choose a total emission measure for our simulations, we conducted a number of three-temperature fits to the spectrum of ζ Pup, using an fixed value of 1.0×10^{22} cm⁻² (c.f., Berghöfer, Schmitt, & Cassinelli 1996) for the interstellar absorption column. These fits resulted in total emission measures in the range $(2.4$ – $5.0) \times 10^{55}$ cm⁻³ (for an adopted distance of 450 kpc, Schaerer, Schmutz, & Grenon 1997) depending on whether we tried to fit the nitrogen lines or the oxygen lines (this discrepancy is discussed in more detail in Paper II) and we chose a value of 3.6×10^{55} cm⁻³ for the total emission measure. For the constant DEM distribution, this implies a DEM value of 1.0×10^{55} cm⁻³. For our simulated exposure time, we used 68,598 s, the exposure time of our observation of ζ Pup. For all of the simulations, n_e was taken to be 8×10^{13} cm⁻³. We chose this particular density value

¹actually one component for each of the database’s temperature values, with each component having the same emission measure

because it is large enough so that, like in the actual stellar spectra, the forbidden lines of the helium-like triplets are completely pumped into the intercombination lines. For the simulated line profiles we used the ISIS thermal/turbulent line profile function:

$$\phi_{Z,z,i}(\lambda) = \frac{1}{\sigma_{Z,z}\lambda_{Z,z,i}\sqrt{2\pi}} \exp\left(\frac{(\lambda/\lambda_{Z,z,i} - (1 + v_r/c))^2}{2\sigma_{Z,z}^2}\right) \quad (16)$$

where

$$\sigma_{Z,z} \equiv c^{-1} \left(\frac{1}{2}v_t^2 + \frac{kT_{p,Z,z}}{m_Z} \right)^{1/2} \quad (17)$$

where m_Z is the mass of element Z , k is Boltzmann's constant. We took v_r to be 0 and v_t to be 800 km s^{-1} , approximating the line widths observed by Kahn et al. (2001) for ζ Pup.

3.2. Application of the Method to the Simulated Data

We fit the simulated spectra using the method described in §2.2. In our analysis we do not attempt to use measurements of the continuum to constrain the DEM distribution. However, in order to fit spectra and obtain accurate constraints from the emission lines, it is necessary to account for the continuum. The continuum emission from a collisional plasma is due primarily to bremsstrahlung, though radiative recombination continua and two-photon continua also contribute. For our fits, we use a continuum consisting of three bremsstrahlung components with variable temperatures and normalizations. In all cases, this provides a sufficient empirical representation of the continuum. For the fit model line profiles, we use the same function as for the simulation model line profile (equation 16). However, in the fit, the values of v_r and v_t are taken to free but to have the same values for all lines. Also, in the fit spectral models, we included the same absorption ($1.0 \times 10^{22} \text{ cm}^{-2}$) used for the simulation.

Though we use the same atomic database for the simulations and the model we fit to the simulated data, this does not amount to fitting the data with the same model used for the simulation. For the simulations, the line luminosities are given by equation 3 with $\mathcal{D}(T)$ constant or proportional to $\delta(T - T_{\text{sim}})$ where T_{sim} is the temperature of the simulated plasma. On the other hand, in the model fit to the simulated data, the line luminosities are given by equation 5. Unless all of line power functions have the same shape every other line power function of the same ion, the line luminosities of the simulation model and the fit model will necessarily differ. Therefore, the fits to the simulated data test whether or not the differences in line power shapes between lines of individual ions are small enough for our method to be valid.

We simultaneously fit both the HEG and MEG simulated data to find the best fit values of $D_{Z,z}$ and $n'_{Z,z}$ for each of the ions by minimizing the Cash (1979) statistic. This statistic, unlike the χ^2 statistic, is valid in the regime where the number of counts in a channel is small such as is the case for several of our data sets. We search for a minimum of the Cash statistic with ISIS, first by using its implementation of the Levenberg-Marquardt algorithm and then using its implementation of the simplex algorithm. We then search for confidence intervals, again using ISIS, on the parameters v_r , v_t , and on each of the values of $D_{Z,z}$ and $n_{Z,z}$. In searching for confidence intervals, only the Levenberg-Marquardt algorithm is used. In searching for confidence intervals, a new minimum is frequently found, requiring the process to be restarted. On our workstations (with clock speeds of order 1 GHz), fitting and finding all of these confidence intervals for one of our data sets generally takes a few weeks.

In Figure 2 we plot the best fit values of D as a function of T_p for each of the ions (indicated by filled circles) and also the simulated data and best fit model spectrum. In the plot of D vs. T_p , a diamond surrounds each filled circle. The vertical extent of a diamond indicates the statistical error on the best-fit value of D (given by $\Delta C = 2.706$, where C is the Cash fit statistic — this is the 90% confidence region) and the extent of a diamond to the left and right is given by $\Delta_- \log T$ and $\Delta_+ \log T$, respectively. These temperature ranges are the temperature ranges for which the values of $D_{Z,z}$ represent the approximate average values of the DEM. While we do not assess the quality of the spectral fit quantitatively, it may be seen that the fit is quite good. The fact that the data points in the first panel are consistent with $\mathcal{D} = 1.0 \times 10^{55} \text{ cm}^{-3}$ and the residuals are no larger than the square root of the number of counts indicates that our method is valid. In Figure 3, we show the plots of $D_{Z,z}$ for the simulated spectra of single-temperature plasmas, except for the simulated $3 \times 10^5 \text{ K}$ plasma spectrum which had only a few counts. The fits for these spectra, which we do not show, are also quite good. In the first panel of Figure 2 and in Figure 3 we use the same temperature range on the horizontal axis and 3 orders of magnitude in DEM on the vertical axis. This allows slopes of lines in the various plots to be compared. Our best-fit values of v_r and v_t have uncertainties of a few tens of km s^{-1} and are consistent with the input values of zero and 800 km s^{-1} , respectively.

It may be seen from Equation 3 that, for a constant DEM distribution, we expect the values of $D_{Z,z}$ to be that constant value of the DEM and, as illustrated in the first panel of Figure 2, within the errors, this is indeed what we find. This, and the good quality of the fits indicates that the fact that not all of the power functions of every ion have the same temperature dependence does not cause our method to be significantly inaccurate. As our simulated plasma has only a single density, this does not test whether or not deviations in the line power functions from the form of Equation 11 cause significant inaccuracies in our DEM determinations. Using plasmas with distributions of densities would have provided a

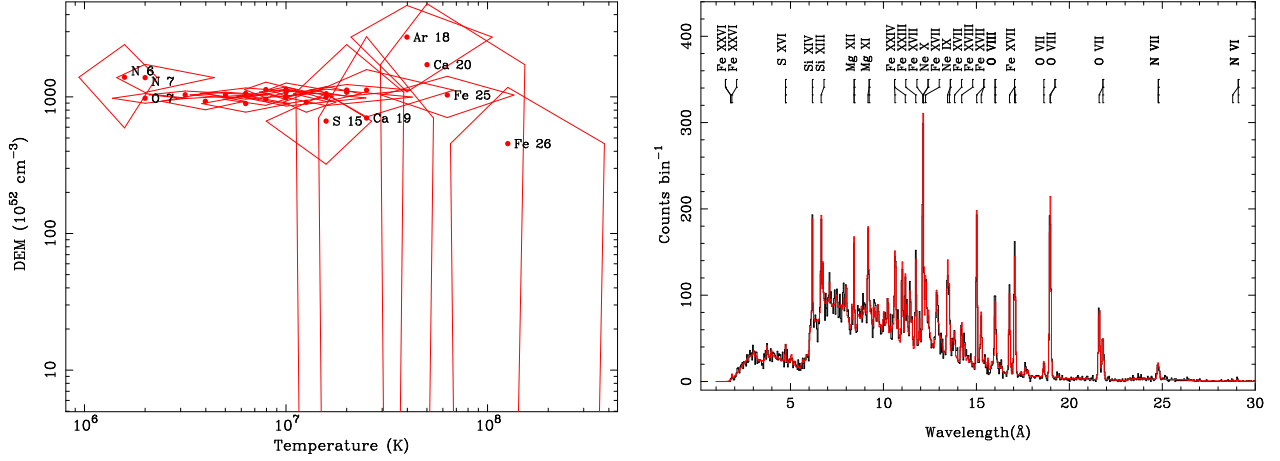


Fig. 2.— In the first panel, the results for the simulated data for a DEM constant in the range 3.2×10^5 – 7.9×10^8 K ($\mathcal{D} = 1.0 \times 10^{55}$ cm $^{-3}$) is plotted. For each ion Z, z , we plot a filled circle at $(T_{p,Z,z}, D_{Z,z})$ where $D_{Z,z}$ is our best-fit value. The vertical extent of the diamond around a filled circle indicates the confidence region determined for $D_{Z,z}$ and the horizontal extent of a diamond is given by $\Delta_- T_{Z,z}$ and $\Delta_+ T_{Z,z}$, which is defined in the text and is, approximately, the region over which the ion emits. The ions corresponding to the data points are labeled using Arabic numerals rather than Roman numerals. Because the data points are so close in this plot, we label only a few of them. In the second panel we show the simulated MEG spectrum (black) and the best-fit model obtained with our method (red). We label several bright lines. Though we do not show it here, the HEG spectrum was also used in the fit. For this and all of our simulated spectra, we adopt the absorption column (1.0×10^{20} cm $^{-2}$), total emission measure (3.6×10^{55} cm $^{-3}$) emission measure, and line width (800 km s $^{-1}$) of ζ Pup. The fact that the data points in the first panel are consistent with $\mathcal{D} = 1.0 \times 10^{55}$ cm $^{-3}$ and the residuals are no larger than the square root of the number of counts indicates that our method is valid.

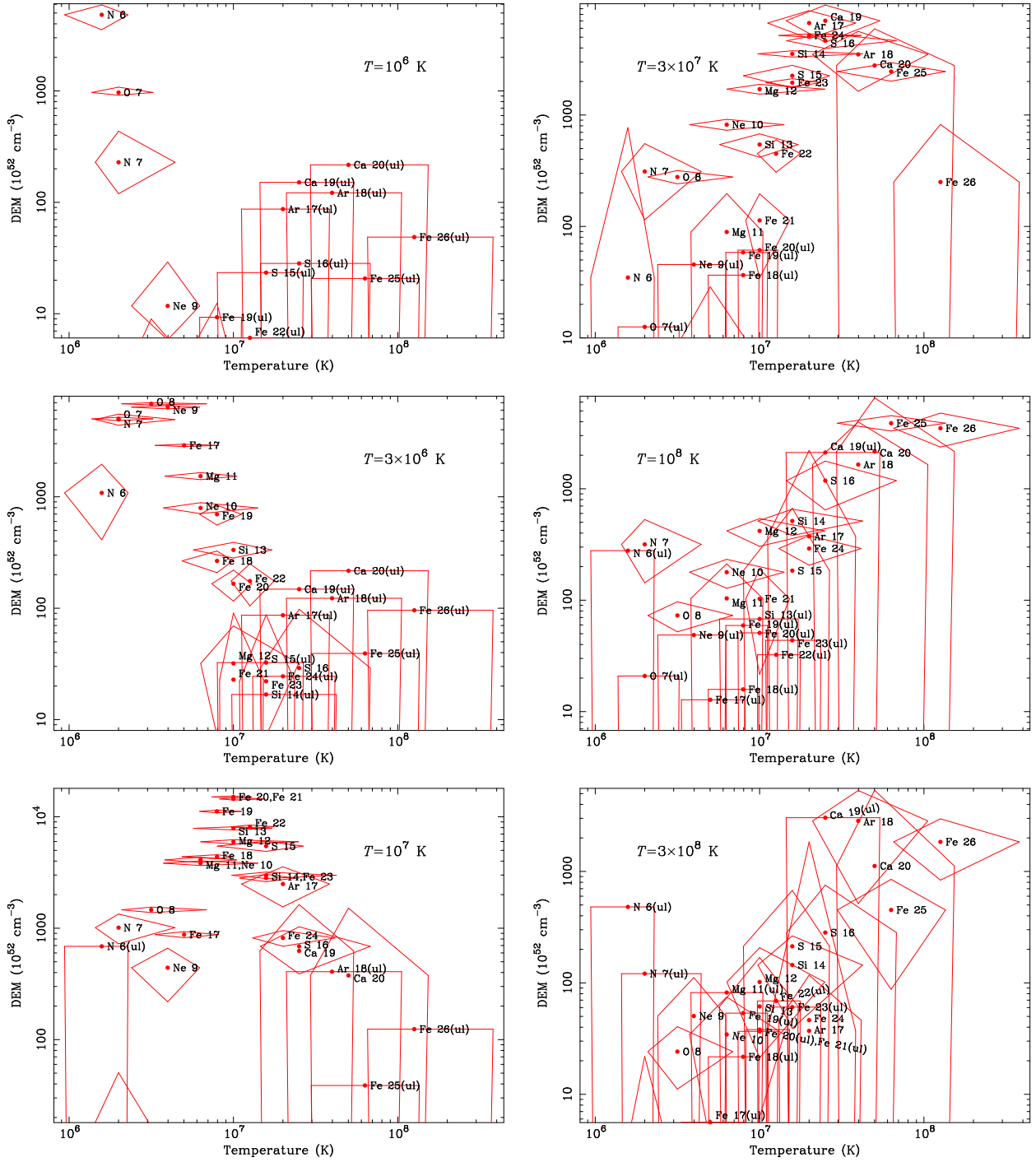


Fig. 3.— Plots of DEM constraints for spectra of plasmas at the single temperatures 10^6 , 3×10^6 , 10^7 , 3×10^7 , 10^8 , and 3×10^8 K. The designation “(ul)” indicates an upper limit.

test of this. However, this would not have provided a test of the accuracy of our method for plasmas with strong ambient radiation fields. Simulating the emission of a plasma with an ambient radiation field is beyond the scope of this work.

For each of the single temperature simulations, the determined values of $D_{Z,z}$ show a peak at the temperature of the simulated plasma. However, the sharpness of the peak differs for each of the simulations. These plots may be understood as “temperature-spread functions” in analogy with point spread functions in images for use in evaluating our results from observed spectra.

4. Discussion

We have described a method for deriving constraints on the differential emission measure distribution of a collisionally ionized plasma from its X-ray emission spectrum and displaying these constraints in a way that indicates the DEM distribution. We have designed our technique to account for the line pumping that occurs at high densities and with high radiation intensities. We have applied our method to simulated spectra and demonstrated that, with this method, we can recover simulated DEM distributions in, approximately, the temperature range 10^6 – 3×10^8 K from their emission line spectra subject to a temperature resolution comparable to the width of the line power functions: a few tenths of a decade.

We expect that the technique described here will be useful in the analysis of high-resolution spectra of plasmas in collisional ionization equilibrium in several astrophysical contexts. This technique is particularly useful in cases where lines are broadened to the point of being blended. Therefore, we expect this technique to be especially useful in the analysis of the X-ray spectra of hot stars and we apply it to spectra of nine hot stars in Paper II. Mukai et al. (2003) have shown that the X-ray spectra of some cataclysmic variable stars are characteristic of plasmas in collisional ionization equilibrium. Some of those spectra show lines as broad as 500 km s^{-1} . Therefore, this technique may be useful in the analysis of those objects. Even for spectra in which lines are not broad and blended, this technique has advantages over others. It does not require fitting of individual lines to determine their fluxes and is therefore easily automated. Also with this technique, it is not necessary to make assumptions or introduce biases about the form of the DEM distributions. Therefore, our technique may also be useful for analysis of high-resolution spectra of the coronae of cool stars obtained with *XMM-Newton* and *Chandra*. The *Astro-E II* observatory will be able to obtain high-resolution spectra of extended objects. Therefore, with the data from that observatory, our technique may be useful in the analysis of the spectra of clusters of galaxies and halos of elliptical galaxies. The fact that this algorithm can be easily automated

may be of particular importance when the DEM distributions need to be determined for a large number of spectra. The fact that the anticipated *Constellation-X* observatory will have a very large effective area for high-resolution spectroscopy will enable it to obtain spectra for a large number of objects that are too faint to be efficiently observed with the three previously mentioned observatories. Therefore, our technique may be especially useful in the analysis of the large number of high-resolution X-ray spectra that will be obtained with that observatory.

We thank John Houck for assistance implementing our analysis technique in ISIS, Dan Dewey for a careful reading of the manuscript, and the referee, Ehud Behar, for helpful comments. Support for this work was provided by the National Air and Space Administration (NASA) through Chandra Award Number GO0-1119X by the Chandra X-ray Observatory Center (CXC) which is operated for and on behalf of NASA by the Smithsonian Astrophysical Observatory (SAO) under contract NAS8-39073. Support for this work was also provided by NASA through contract NAS8-01129 and by the SAO contract SVI-61010 for the CXC.

REFERENCES

- Behar, E., Cottam, J., & Kahn, S. M. 2001, *ApJ*, 548, 966
- Berghöfer, T. W., Schmitt, J. H. M. M., & Cassinelli, J. P. 1996, *A&AS*, 118, 481
- Brinkman et al. 2001, *A&A*, 365, L324
- Cash, W. 1979, *ApJ*, 228, 939
- Kahn, S. M., Leutenegger, M. A., Cottam, J., Rauw, G., Vreux, J.-M., den Boggende, A. J. F., Mewe, R., & Güdel, M. 2001, *A&A*, 365, L312
- Mewe, R., Gronenschild, E. H. B. M., & van den Oord, G. H. J. 1985, *A&AS*, 62, 197
- Mukai, K., Kinkhabwala, A., Peterson, J. R., Kahn, S. M., & Paerels, F. 2003, *ApJ*, 586, L77
- Paerels, F. B. S. & Kahn, S. M. 2003, *ARA&A*, 41, 291
- Pottasch, S. R. 1963, *ApJ*, 137, 945
- Raymond, J. C. & Smith, B. W. 1977, *ApJS*, 35, 419
- Sako, M., Liedahl, D. A., Kahn, S. M., & Paerels, F. 1999, *ApJ*, 525, 921

Schaerer, D., Schmutz, W., & Grenon, M. 1997, ApJ, 484, L153

Smith, R., Brickhouse, N., Liedahl, D., & Raymond, J. 2002, at
http://asc.harvard.edu/atomdb/features_density.html

Smith, R. K., Brickhouse, N. S., Liedahl, D. A., & Raymond, J. C. 2001, ApJ, 556, L91